Dynamic Docking of Myosin and Actin Observed with Resonance Energy Transfer[†]

Douglas D. Root,* Shaun Stewart, and Jin Xu

University of North Texas, Department of Biological Sciences, Division of Biochemistry and Molecular Biology, P.O. Box 305220, Denton, Texas 76203-5220

Received October 18, 2001; Revised Manuscript Received December 9, 2001

ABSTRACT: Atomic models of myosin subfragment-1 (S1) and the actin filament are docked together using resonance energy-transfer data from both pre- and postpowerstroke conditions. The quality of the resulting best fits discriminated between neck-region orientations of the S1 for a given set of experimental conditions. For measurements of the postpowerstroke states in the presence of ADP, resonance energy-transfer data alone are sufficient to dock the atomic models and provide evidence that S1 exists with at least two neck-region orientations under these conditions. To dock the prepowerstroke state, resonance energy-transfer data were used in combination with previous chemical cross-linking data to determine that a neck-region orientation similar to that of a proposed prepowerstroke state best fit the data. The resulting models determined independently from electron microscopy compare favorably with micrographs from the recent literature. The docking models by resonance energy transfer suggest that the larger movements in the light-chain binding domain are accompanied by twisting and rotating movements of the catalytic domain, causing a tilt of approximately 30° during the weak-to-strong transition. This transition provides the displacement necessary to support motility and force generation.

The molecular description of the contractile process in muscle is a key goal for the detailed understanding of motility and its relationship to numerous pathogenic conditions. Atomic resolution models of myosin subfragment-1 (S1) bound to actin in the absence of ATP have been assembled from electron micrographs, crystallographic atomic models, and X-ray diffraction of aligned actin filaments (*1*−*4*). These models have largely used the earliest atomic model of skeletal myosin S1 for the docking of myosin onto actin (*2*, *4*). More recently, new atomic models of myosin S1 have been determined that have highly divergent neck-region orientations (*5*, *6*). The light-chain binding domains in the smooth muscle S1 and the ADP-bound scallop muscle S1 are oriented in nearly opposite directions to each other, while the light-chain binding domains of the other crystal structures are more intermediate in their orientations. The discovery of these new structures begs the question, is there any physical evidence that each of these or closely related structures exist when S1 is bound to actin?

The possibility that these structures represent different stages in the actomyosin ATPase cycle has been proposed in different forms (*5*, *7*, *8*). The actomyosin cycle is described as a process of cyclic interactions between myosin and actin that is guided by the transitions of myosin between weak and strong actin binding states. The weak binding state is hypothesized to exist as or be a prelude to a prepowerstroke conformation of S1 on actin and can be mimicked by the use of phosphate analogues that bind with ADP to myosin. Spectroscopic studies report a greater disorder of the myosin head orientations in the weak binding state that change in average orientation by just over 30° during conversion to the strong binding state (*9*). As the strong binding state follows from the weak binding state, a strain develops that results in the force driving displacement between the filaments. If the terminal postpowerstroke conformation of S1 and actin were compared to the prepowerstroke conformation, one could measure the contributions of the different structural orientations and calculate the overall displacement that occurs. Some proposed models designate the orientation of the neck region found in the smooth muscle S1 atomic model as a prepowerstroke conformation and those of the skeletal muscle S1 or related scallop muscle S1 structures as postpowerstroke conformations (*5*, *7*, *8*). The overall displacement associated with the powerstroke depends on the orientations of these structures on the actin filament. The determination of these orientations requires the docking of the existing atomic models of myosin onto actin.

The previous docking of atomic models has relied primarily on data from electron microscopy (EM)[1] three-dimensional reconstructions (*2*). While the strong binding states are relatively easier to identify by cryo-EM producing nominal resolutions to just under 2 nm, glimpses of the

[†] We gratefully acknowledge support from the National Institutes of Health Grant No. AR44737.

* Corresponding author. Phone: 940-565-2683. Fax: 940-565-4136. E-mail: DROOT@UNT.EDU.

[1] Abbreviations: CY3, trademark name for 1-(ϵ-carboxypentyl)-3,3,3′,3′-tetramethylindocarbocyanine-5,5′-disulfonate potassium salt *N*-hydroxysuccinimide ester; DEAE, diethylaminoethyl anion exchange chromatography; DMSO, dimethyl sulfoxide; DTNB, 5,5′-dithio-bis-(2-nitrobenzonic acid); DTPA, diethylenetriaminepentaacetic acid; *E*, efficiency of energy transfer; EM, electron microscopy; FPLC, fast protein liquid chromatography; *L*, loss function; MALDI-TOF, matrix-assisted laser desorption ionization time-of-flight mass spectroscopy; pepRPC, reversed-phase chromatography column; PH, tetramethyl-rhodamine-phalloidin; RET, resonance energy transfer; RLC, regulatory light chain; S1, myosin subfragment-1; RMSD, root-mean-squared difference; TEA, triethylamine acetate; *J*, overlap integral; κ^2, orientation factor; η, index of refraction; ϕ_D, quantum yield of the donor; *R*, separation distance; R_0, critical transfer distance; τ, fluorescence lifetime.

10.1021/bi015869o CCC: $22.00
Published on Web 01/17/2002

prepowerstroke state at less optimal resolutions have been reported from insect flight muscle (*10*). Two-dimensional electron micrographs of myosin V have provided further clues to the nature of the pre- and postpowerstroke conformations of the myosin head on actin (*11*). These studies indicate substantial changes in the orientation of the light-chain binding domain, with less rotation of the catalytic domain on actin. Atomic models from higher resolution structural data of the prepowerstroke state of S1 on actin would provide a clearer view of the molecules in the step-generating transitions.

Alternatively, biochemical and spectroscopic structural measurements can be used independently from EM to dock atomic models at high resolution. Chemical cross-linking identifies direct contacts, even if they might be transient. The recent luminescence resonance energy-transfer (RET) method provides quantitative measurements of distant proximities between specific labeled sites, even between transiently interacting molecules (*8*). These techniques significantly improve upon conventional RET used previously for structural determinations (*12*, *13*).

In this paper, the possible contribution of a catalytic domain rotation in addition to the reorientation of the neck region is tested using RET measurements and molecular modeling. Methods are developed to dock atomic models of S1 onto actin filaments using RET measurements or chemical cross-linking data. New RET data are collected and pooled with previously published RET and chemical cross-linking data to provide a sufficient database to generate unique fits of existing atomic models of S1 onto models of F actin. For the first time, both pre- and postpowerstroke states of S1 using ADP and transition-state analogues were docked onto actin. The resulting models are compared to electron micrographs and previous atomic models of S1 on actin. They demonstrate excellent agreement with postpowerstroke state models while providing potentially enhanced resolution and reveal a unique transitional form of the prepowerstroke state.

MATERIALS AND METHODS

Organic Synthesis and Reagents Used. The RET donors were freshly synthesized terbium chelates with a cytosine-enhancing ligand and functional groups for the specific protein labeling. Three functional groups were attached: (1) anhydrides to label the N-terminal residues of RLC, (2) ethylenediamine to label Gln41 on actin, or (3) maleimide to react with myosin Cys707 or actin Cys374. The RET acceptor probes were versions of conventional fluorophores to specifically label the myosin nucleotide site, the N-terminal residues of RLC, actin Cys374, or the phalloidin binding site. Procured reagents included CY3 (Amersham Pharmacia Biotech, Piscataway, NJ), terbium chloride hexahydrate, cytosine (Aldrich, Milwaukee, WI), tetramethylrhodamine-phalloidin, papain, maleimide, DTNB, ATP, sodium orthovanadate, beryllium, aluminum chloride, sodium fluoride, DTPA (Sigma, St. Louis, MO), 5-aminotetramethylrhodamine, (Research Organics, Cleveland, OH), and fluorescein-5-maleimide (Molecular Probes, Eugene, OR).

CY3−maleimide was prepared by combining 0.1 mM monoreactive CY3 with 1 mM 2-aminoethylmaleimide (Molecular Probes) in 0.1 M sodium phosphate (pH 7.8) for 1 h. The mixture was immediately diluted 10-fold with 50 mM TEA (pH 7.0) and loaded on a pepRPC column equilibrated with 50 mM TEA (pH 7.0), and after unreacted 2-aminoethylmaleimide eluted from the column, a step gradient to 100% methanol was used to elute the CY3 in a single sharp peak which was collected and dried. CY3−ATP was prepared as previously described (*14*).

An ethylenediamine-modified cytosine terbium chelate was synthesized by incubating 10 mM cytosine with 10 mM DTPA in DMSO for 1 h, followed by the addition of ethylenediamine to 0.1 M for 1 h. The mixture was dissolved in running buffer and then separated by a DEAE Sepharose fast flow FPLC. The ethylenediamine-modified cytosine terbium chelate eluted with 60 mM NaCl and 20 mM phosphate (pH 6.5). The structure of the ethylenediamine-modified cytosine terbium chelate was verified by MALDI-TOF mass spectroscopy and also by reactivity with fluorescamine. The concentration of the chelate was determined from titration with a known concentration of terbium, and the molar extinction coefficients of $E_{243\,nm} = 20\,000\ M^{-1}\ cm^{-1}$ and $E_{295\,nm} = 9300\ M^{-1}\ cm^{-1}$ were measured.

A maleimide-modified cytosine terbium chelate was synthesized by incubating 10 mM cytosine with 10 mM DTPA in DMSO for 1 h, followed by the addition of 2-aminoethylmaleimide to 0.1 M for 1 h. The mixture was dissolved in running buffer and then separated by a DEAE Sepharose fast flow FPLC. The structure of the maleimide-modified cytosine terbium chelate was verified by MALDI-TOF mass spectroscopy. The reactivity of the maleimide was determined by incubation with an equal molar concentration of 2-mercaptoethanol, followed by assaying the remaining mercaptoethanol with DTNB. Typically, more than 50% reactivity was retained.

Protein Labeling. Rabbit skeletal myosin was prepared by the method of Godfrey and Harrington (*15*). S1 was digested from myosin with papain and separated according to Weeds and Pope (*16*). The protein concentrations were determined using absorbance coefficients at 280 nm of 0.55, 0.60, and 0.75 $(mg/mL)^{-1}\ cm^{-1}$ for myosin, RLC, and S1, respectively, and at 290 nm of 0.63 $(mg/mL)^{-1}\ cm^{-1}$ for actin.

DTNB dissociated RLC from rabbit skeletal myosin and the RLC was collected by ethanol precipitation and Superdex 75 FPLC (*14*, *17*). The purified RLC was labeled either with a cytosine−DTPA terbium chelate as described previously (*18*) or by aminotetramethylrhodamine−DTPA prepared in a similar fashion but with aminotetramethylrhodamine used in place of cytosine. The labeled RLC was exchanged back into S1 by first dissociating bound RLC with 0.5 M KCl, 2 mM EDTA, and 10 mM imidazole (pH 8.0) and separating the stripped S1 by Superdex 75 gel filtration. The labeled RLC was immediately exchanged into the S1 in 0.5 M NaCl, 5 mM $MgCl_2$, and 10 mM imidazole (pH 8.0) and separated from free RLC by Superdex 75 FPLC. Titration of the exchanged S1 with known concentrations of terbium indicated that approximately 20% of the S1 was labeled with the cytosine−DTPA RLC (originally 95% labeled). In other experiments, UV−vis spectroscopy indicated that approximately 5% of S1 was labeled when exchanged with aminotetramethylrhodamine−DTPA RLC (originally 21% labeled).

In different experiments, either the maleimide-modified cytosine terbium chelate or the CY3−maleimide at 50 μM was reacted with approximately 10 μM F-actin in 0.1 M KCl,

Table 1: Mapping the Labeling of Gln41 (Q41) on Actin with a Terbium Chelate

cyanogen bromide fragment sequence of actin	Q41	Q	C	W	Y
DEDETTALVCDNGSGLVKAGFAGDDAPRAVFPSIVGRPRHQGVM	Y	Y	Y	N	N
VGM	N	N	N	N	N
GQKDSYVGDEAQSKRGILTLKYPIEXGIITNWDDM	N	Y	N	Y	Y
EKIWHHTFYNELRVAPEEHPTLLTEAPLNPKANREKM	N	N	N	Y	Y
TQIM	N	Y	N	N	N
FETFNVPAM	N	N	N	N	N
YVAIQAVLSLYASGRTTGIVLDSGDGVTHNVPIYEGYALPHAIM	N	Y	N	N	Y
RLDLAGRDLTDYLM	N	N	N	N	Y
KILTERGYSFVTTAEREIVRDIKEKLCYVALDFENEM	N	N	Y	N	Y
ATAASSSSLEKSYELPDGQVITIGNERFRCPETLFQPSFIGM	N	Y	Y	N	Y
ESAGIHETTYNSIM	N	N	N	N	Y
KCDIDIRKDLYANNVM	N	N	Y	N	Y
SGGTTM	N	N	N	N	N
YPGIADRM	N	N	N	N	Y
QKEITALAPSTM	N	Y	N	N	N
KIKIIAPPERKYSVWIGGSILASLSTFQQM	N	Y	N	Y	Y
WITKQEYDEAGPSIVHRKCF	N	Y	Y	Y	Y

2 mM $MgCl_2$, and 10 mM imidazole (pH 7.0) at 4 °C overnight (*8*). Centrifugation and subsequent dialysis of the F-actin separated it from unreacted reagent. After recycling of the actin back to its monomeric form as verified by ultracentrifugation at 100 000*g* for 1 h, the actin was repolymerized.

Enzymatically catalyzed labeling of actin at Gln41 with the ethylenediamine-modified cytosine terbium chelate followed standard procedures used for other ethylenediamine-modified probes (*19*). The efficiency of the actin labeling was measured to be 79−100% in separate labeling experiments. The modification was mapped using cyanogen bromide cleavage of the labeled actin and isolation of the labeled fragment by reversed-phase FPLC. Measurement of cysteine reactivity with fluorescein-5-maleimide at pH 7 and the lack of detectable tryptophan or tyrosine fluorescence verified that the labeled peptide was the fragment containing Gln41 (see Table 1).

RET. RET measurements were determined by methods described previously (*20*). Lifetime measurements were used to determine the efficiency of RET (E) for the distance (R) between the donor and the acceptor according to the equation

$$E = 1 - \tau_{da}/\tau_{d} = \sum_{i}(R_0^6/R_i^6)/(1 + \sum_{i}(R_0^6/R_i^6)) \quad (1)$$

In this equation, τ_{da} is the apparent long-lived lifetime of the acceptor in the presence of the donor, τ_{d} is the lifetime of the donor in the absence of acceptor, and R_0 is the critical transfer distance. The critical transfer distance was calculated according to the equation

$$R_0 = (8.79 \times 10^{-11}\, J\kappa^2\eta^{-4}\phi_{D})^{1/6}\ \text{nm} \quad (2)$$

In this equation, J is the calculated overlap integral for the acceptor with terbium and has values of 9.3×10^{14}, 3.6×10^{15}, and 5.1×10^{15} for fluorescein-5-maleimide, tetramethylrhodamine, and CY3, respectively; κ^2 is the dynamic average value of the orientation factor, $^2/_3$; $\eta = 1.4$ is the refractive index of the medium; and $\phi_D = \tau_d/4.75$ ms is the quantum yield of the donor (*18*, *20*). Uncertainty in the orientation factor will cause, at most, a 10% error in the separation distance, because terbium has an isotropic emission, and this error is comparable to or less than other sources of error in the measurements of this study (*21*). The effects of the sizes of probes used in this study have been examined on model compounds that indicate a typical error of approximately ±0.5 nm (*20*). The distances from the α carbons of myosin models were measured to the appropriate side-chain atoms of actin for the docking calculations, so the probe size error might be slightly larger due to the uncertainty in myosin side-chain orientations. The RET measurements were performed in 0.1 M KCl, 2 mM $MgCl_2$, and 10 mM imidazole (pH 7.0). The S1 concentrations were 0.5−2.0 μM, and equal molar actin was used.

Calculation of Molecular Docking Models. The RET efficiency measurements were compared with atomic models of S1 on F-actin by calculating the expected RET efficiency for each atomic model (Figure 1). The calculation of the RET efficiency, as described in eq 1, took into account the multiple acceptors per donor due to the polymeric structure of actin. The difference between the RET efficiencies measured experimentally (E_{exp}) and those calculated from atomic models (E_{calcd}) were used to generate a loss function, L:

$$L = \sum_{i}(E_{exp} - E_{calcd})^2/\sigma_i^2 \quad (3)$$

The squared difference was normalized to the standard deviation squared (σ^2) based on at least three measurements.

The docking of S1 on actin was guided by minimizing the loss function in a computational fitting process. Rotation and translation matrices corresponding to specific rotations around or translations along the *X*, *Y*, and *Z* axes of the S1 atomic models were applied in Microsoft Excel. The solver function using a quasi-Newtonian algorithm determined the parameters for rotating the models following each iteration until the best fit was achieved. Macros were written to export the coordinates generated in the spreadsheet to PDB format for viewing with RASMOL.

For postpowerstroke (ADP) data, only RET data were used for docking purposes. When the prepowerstroke (ADP·AlF_4) data were fit, chemical cross-linking data between the N-terminus of actin and the lysine-rich region on S1 were also used, because RET data did not produce a unique fit on its own. These regions can be cross-linked by EDC in the enzymatically active complex of acto−S1 (*22*, *23*). Specifically, the average coordinates of the α carbons from the four amino terminal residues of actin were constrained to

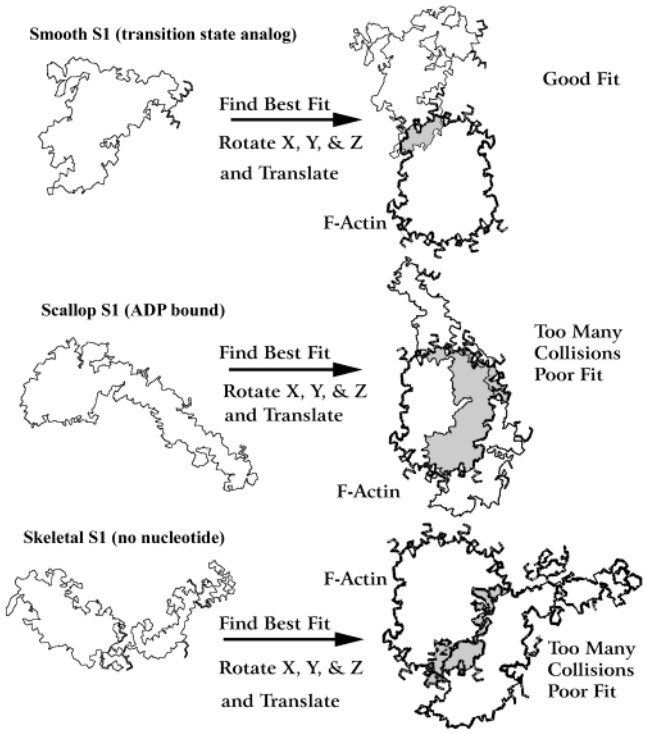

FIGURE 1: Illustration of how docking models were determined. Each available atomic model of S1 from three different states, as shown at the left, were docked independently onto an atomic model of the actin filament using the same RET data. The best fit of each atomic model of S1 on actin was determined by computer automated rotation and translation of the model until a minimal loss function was obtained (eq 3). On the right, outlines of the three best-fit models to the ADP·AlF_4 data were obtained; however, only the smooth muscle S1 model had a tolerable amount of collisions with actin and was selected as the overall best model. Similar procedures were performed for RET data collected in the presence of other nucleotide analogues. The shaded regions indicate regions of contact or overlap between the S1 model and the actin filament that is oriented perpendicular to the page.

be within 1 nm of the approximate location of the lysine-rich region on S1. The lysine-rich region location, which is flexible in the crystal structures, was estimated on the basis of the average of the position between the two nearest α carbon coordinates present in the crystallographic atomic model.

Labeling sites on the different atomic models of S1 were determined by multiple alignment of the sequences using MACAW software (Figure 2). The position of the N-terminus of RLC was determined by combining published RET measurements with our own data and using a triangulation method on the skeletal muscle S1 atomic model (*13*, *14*). The α carbon coordinates of the homologous S1 residues were used to approximate the probe locations in the different S1 species.

The probe sites on actin were approximated by using the coordinates of appropriate side-chain atoms that are fluorescently labeled, because no variations in the amino acid sequence are present in the actin models tested. The residues Cys374 and Gln41 were labeled directly; however, the phalloidin binding site was inferred from published photocross-linking data to a modified phalloidin (*24*). The coordinates of residue Glu117 was used for docking purposes, because it should best approximate the position of a fluorophore on the bound phalloidin.

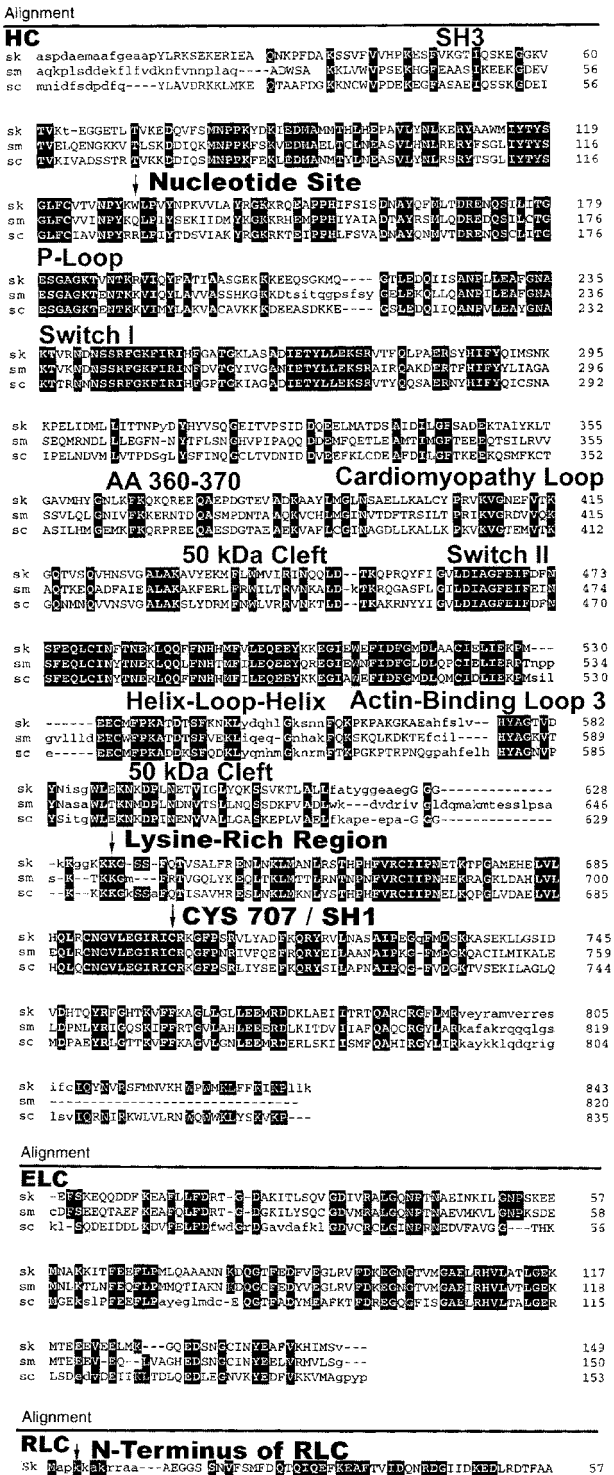

FIGURE 2: Multiple sequence alignment of skeletal, smooth, and scallop muscle myosins used for the docking. Approximately 40% of the residues are identical across all three structures, with the greatest amount of identities in the heavy-chain (HC) region. Still higher degrees of identity are found between any pair of structures, with most of the differences being conservative substitutions. Sequence alignments were performed using MACAW software. The labeling sites used for RET are indicated. Also shown are some of the key structural features of myosin.

RESULTS

These experiments use RET assisted by chemical cross-linking data to generate docking models of different myosin states bound to actin (Figure 1). First, new RET measurements between actin and S1 were collected and combined with our previous measurements to generate a pool of data that was sufficiently large for mathematical modeling. Calculated efficiencies of RET from each atomic model were compared to the experimental data to guide the docking process by a quasi-Newtonian search method. Best-fit models were evaluated for their plausibility based on the resulting loss function and the amount of contacts or collisions between the docked molecules. No constraints to prevent collisions were included during the actual docking simulations. After the new models were determined, they were compared with electron micrographs, because these atomic models are generated independently from the electron micrographs.

RET Data. To acquire RET efficiencies between probes on actin and S1 in the presence of nucleotide analogues that weaken their binding, lifetimes of the sensitized emission were used to isolate the signal from the transient complex. In these RET experiments, there is no time-resolved fluorescence from the acceptor unless energy is transferred to it from the slowly decaying lanthanide donor (*21*). The apparent long lifetime of the sensitized emission of the acceptor reports the lifetime of the quenched donor. Therefore, the structure of the transient acto−S1 complex can be measured from RET through the elimination of background fluorescence from the dissociated or partially labeled actin and S1 molecules by isolating the time-resolved signals.

In addition to our previously published measurements, new data were collected for this study (see Tables 2 and 3) which included RET measurements from Gln41 on actin to each of three different labeling sites on S1: the nucleotide binding site, Cys707, and the N-terminus of RLC. In addition, RET was measured between Cys374 on actin and myosin Cys707 or the N-terminus of RLC. Furthermore, measurements were made from the phalloidin binding site on actin to Cys707 or the N-terminus of RLC. Our previously published data that aided the docking process included measurements from the N-terminus of RLC to Cys374 on actin or to the nucleotide binding site on myosin (*8*).

Best-Fit Docking Models of Different S1 States. The pre- and postpowerstroke states were simulated with ADP or ADP·AlF_4 bound, respectively (Figures 3 and 4). Results using ADP·BeF_x or ADP·V_i for the prepowerstroke state yielded results similar but not quite identical to those for which ADP·AlF_4 was bound (RMSDs of 0.4 and 1.0 nm, respectively) which gives a rough approximation of the resolution of the docking process. The measurements in the absence of nucleotide were not used for docking experiments, because labeling the nucleotide site of S1 requires the presence of the fluorescently labeled ADP. The measurements from Cys707 were only used for the ADP state, because the modification of this residue might influence transitions to or from the prepowerstroke state (*25*). In the place of this RET data, chemical cross-linking data between the lysine-rich loop and the N-terminus of actin was used as a constraint to dock S1 on actin for the prepowerstroke state (*23*).

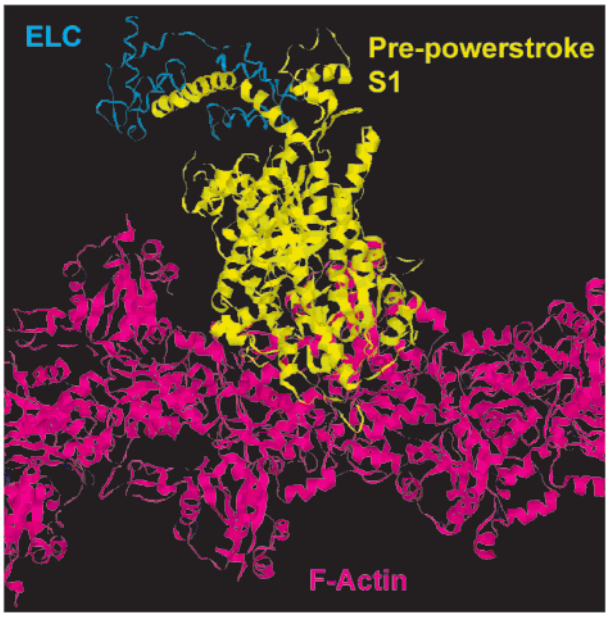

FIGURE 3: Prepowerstroke model of S1 on the actin filament. The smooth muscle S1 atomic model is docked onto refined actin filament using chemical cross-linking data in combination with RET data. The model illustrated is fit with RET data acquired in the presence of ADP·AlF_4. Not shown are closely related models from RET data acquired in the presence of ADP·BeF_x (RMSD = 0.4 nm) and ADP·V_i (RMSD = 1.0 nm). The actin filament is oriented parallel to the page at the bottom of the figure.

Three atomic models of S1 were docked to actin using the RET data (Figure 1). The best-fit model for each state was determined and then evaluated based on the loss function, the distance between the N-terminus of actin and the lysine-rich region on myosin, and the plausibility of any collisions at the acto−S1 interface. Of the fits to the RET data from acto−S1 in the presence of ADP, the scallop muscle ADP−S1 atomic model yielded the most plausible result. The skeletal muscle S1 model showed too many collisions with the actin filament (Figure 1), and the smooth muscle S1 model did not make enough contacts with the actin filament to be consistent with a strong binding state. Examination of some of our data raised the possibility that multiple states might coexist in the presence of ADP. Our previous intramolecular measurements between RLC and the nucleotide site on S1 in the presence of actin indicated that an orientation of the light-chain binding domain similar to that of skeletal S1 was present but did not rule out the coexistence of additional neck-region orientations giving weak RET efficiencies (*14*). Taken together, these data suggest that, in the presence of ADP, neck-region orientations similar to skeletal muscle S1 and scallop muscle ADP−S1 coexist on actin. When two states coexist, the state with a significantly higher RET efficiency will dominate the detected signal and may appear to be the only structure present. Therefore, the varying designs in the two experiments can detect the presence of at least two different states, because the alternative geometries are sensitive to different states.

In the presence of phosphate analogues that mimic the prepowerstroke states, only smooth muscle S1 orientation of the neck region produced a plausible best-fit model. The best-fit models of skeletal muscle S1 and scallop muscle ADP−S1 were unrealistically embedded within the actin

Table 2: Comparisons of Calculated Efficiencies from RET and EM Docking Models of S1 on Actin

		postpowerstroke-state data					
sites	RET S1ADP[a]	best fit[b]		EM vis[e]		EM calcd[f]	
actin-S1	to F-actin	refined[c]	initial[d]	refined	initial	tefined	initial
Q41−RLC	0.35 ± 0.07	0.31	0.35	0.03	0.04	0.03	0.04
PH−RLC	0.26 ± 0.04	0.31	0.28	0.03	0.03	0.04	0.04
C374−RLC	0.37 ± 0.03	0.35	0.36	0.05	0.04	0.05	0.03
Q41−NUC	0.67 ± 0.08	0.61	0.61	0.40	0.31	0.34	0.28
C374−NUC	0.37 ± 0.11	0.54	0.52	0.31	0.30	0.29	0.27
Q41−C707	0.54 ± 0.13	0.48	0.59	0.60	0.74	0.52	0.69
PH−C707	0.53 ± 0.14	0.63	0.68	0.61	0.61	0.56	0.57
C374−C707	0.40 ± 0.06	0.40	0.37	0.38	0.33	0.34	0.29
NT−LR[g]	0	1.8 nm	3.2 nm	1.8 nm	1.5 nm	2.4 nm	1.8 nm

[a] Observed RET efficiencies measured in three or more separate experiments with ADP present. [b] Best-fit RET docking models were used to calculate these efficiencies of energy transfer. Typical R_0 values from donor to acceptor were 4.3 nm (from terbium on C707 to fluorescein-5-maleimide on C374), 5.1 nm (from terbium on RLC to tetramethylrhodamine-phalloidin (PH) or from terbium on Q41 to tetramethylrhodamine on RLC), and 5.4 nm (from terbium on RLC to CY3 on C374 or from terbium on C374 or Q41 to CY3−ADP). [c] Refined model of the F-actin filament (*3*) was used for docking. [d] Initial model of the F-actin filament (*1*) was used for docking. [e] Efficiencies calculated from EM docking models that were visually docked (*2*). [f] Efficiencies calculated from computationally docked EM docking models (*4*). [g] Approximate distances between actin's N-terminus and the lysine-rich region in each model.

Table 3: Comparisons of RET Efficiencies from RET Docking Models and Observed Measurements

	prepowerstroke-state data								
sites	RET[a]	refined[b]	initial[c]	RET	refined	initial	RET	refined	initial
actin−S1	ADP·AlF_4	AlF_4	AlF_4	ADP·BeF_x	BeF_x	BeF_x	ADP·V_i	V_i	V_i
Q41−RLC	0.50 ± 0.11	0.54	0.45	0.50 ± 0.04	0.51	0.49	0.38 ± 0.08	0.40	0.36
PH−RLC	0.30 ± 0.04	0.36	0.38	0.27 ± 0.05	0.40	0.41	0.22 ± 0.05	0.33	0.32
C374−RLC	0.63 ± 0.06	0.49	0.50	0.66 ± 0.05	0.52	0.53	0.52 ± 0.09	0.45	0.31
Q41−NUC	0.76 ± 0.06	0.75	0.71	0.80 ± 0.01	0.80	0.80	0.75 ± 0.04	0.67	0.65
C374−NUC	0.43 ± 0.09	0.44	0.58	0.36 ± 0.11	0.48	0.66	0.32 ± 0.11	0.39	0.54
NT−LR[d]	0	1 nm	1 nm	0	1 nm	1 nm	0	1 nm	1 nm

[a] Observed RET efficiencies measured in three or more separate experiments in the presence of the indicated nucleotide analogue. [b] Refined model of the F-actin filament (*3*) was used for docking. Best-fit RET docking models were used to calculate these efficiencies of energy transfer. Typical R_0 values from donor to acceptor were 5.1 nm (from terbium on RLC to tetramethylrhodamine-phalloidin (PH) or from terbium on Q41 to tetramethylrhodamine on RLC), and 5.4 nm (from terbium on RLC to CY3 on C374 or from terbium on C374 or Q41 to CY3−ADP). [c] Initial model of the F-actin filament (*1*) was used for docking. Best-fit RET docking models were used to calculate these efficiencies of energy transfer. [d] Approximate distances between actin's N-terminus and the lysine-rich region in each model.

filament (Figure 1). Intriguingly, the direction of the best-fit smooth muscle S1 model is ideally oriented as a prepowerstroke state with the neck region directed toward the pointed end of the actin filament model. Data from each of the phosphate analogues tested generated a similarly oriented model with only a few minor differences. The ADP·BeF_x data produced the weakest fit of the data sets and might be consistent with a greater heterogeneity of the states under this condition. In each model, the catalytic domain of the prepowerstroke state is rotated relative to the model of the postpowerstroke (ADP) state. This rotation displaces the catalytic domain alone by approximately 3 nm toward the barbed end of the actin filament and could contribute to the powerstroke along with the more pronounced rotations of the neck region.

Comparing Actin Filament Models. Different models of the actin filament were also tested by the fitting process (see Tables 2 and 3). The initial model of the F-actin filament as presented by Holmes et al. (*1*) and the refined model as reported by Lorenz et al. (*3*) both produced reasonable fits to the data. Nevertheless, differences in the quality of the resulting models, as perceived by the loss function and the extent of agreement between the model and various biochemical and EM data, were detected. The refined actin filament generated the most plausible models in each case. Although the initial actin filament model (*1*) produced slightly better fits with the postpowerstroke (ADP) state data than with the prepowerstroke state data, the distances between the lysine-rich region on myosin and the N-terminus of actin in the strong (ADP) binding model were less consistent with chemical cross-linking data than those from the models using the refined actin filament (Table 2). Furthermore, the refined actin filament model produced better fits with the prepowerstroke state data both in terms of the lower loss function and the fewer collisions between actin and S1.

Comparisons with Results from EM. The RET results can be compared with those from EM. Cryo-EM has been used to dock atomic models skeletal muscle S1 on actin in the absence of nucleotide (*2*). Either visual methods (*2*) or best-fit computational methods (*4*) produced slightly different fits to the electron-density map from three-dimensional reconstructions. The expected efficiencies of RET from each of these models was calculated and compared to the measured efficiencies of RET of the postpowerstroke (ADP) state (Table 2).

The position of RLC in the cryo-EM docking models of skeletal muscle S1 was quite distant from the actin filament, so the calculated efficiencies of RET were weaker than observed (Table 2). Greater correlations were found with the RET data between sites on the catalytic domain and actin; however, there were distinct differences. In general, models

from cryo-EM that used the refined actin filament model agreed better with the RET data than those based on the initial model of Holmes et al. (*1*). Furthermore, the original visual docking model (*2*) agreed slightly better with RET data than the calculated fit (*4*), although neither model agreed quite as well with the RET data as the best-fit docking models of scallop muscle ADP−S1 on actin. Notably, the largest degrees of variation between the RET docking models and the EM docking models for the position of the catalytic domain on actin were in the axial location of the head. Because two-dimensional electron micrographs, from which the three-dimensional constructions are generated, are taken longitudinally with respect to the actin filament, it can be argued that the greatest degree of uncertainty could be expected in the azimuthal position of S1 on actin. Nevertheless, the RET docking models largely confirm the location of the catalytic domain in the cryo-EM docking models with a few important refinements.

DISCUSSION

The docking of atomic models generated from X-ray diffraction has been recently used to produce models of the postpowerstroke state of S1 on actin based on electron micrographs. RET is demonstrated as an alternative method for docking atomic models at high resolution and has an advantage that the structures can be measured in liquid solution. Recently, it has been shown that this RET technique can measure structural data on transiently associating molecules that are used here to provide a unique glimpse of the prepowerstroke state of S1 interacting with actin (*8*). The RET docking models described here support many of the fundamental observations from EM. In particular, these data provide support for the theory that the prepowerstroke state corresponds to a neck-region orientation of S1 that is similar to that observed in atomic models of smooth muscle S1 in the presence of transition-state nucleotide analogues (*5*).

RET Versus EM Docking Models. The molecular models based on RET provide an independent view of the acto−S1 interface from that of EM. In these models, the catalytic domain of S1 occupies a slightly adjusted position on actin relative to the cryo-EM docking models under strong binding conditions (*2*). Although cryo-EM has not been used to model the weak binding state, tomographic EM images from insect flight muscle have been used to dock both pre- and postpowerstroke states of the myosin head on actin that imply an axial tilting of the catalytic domain (*10*). A remarkably similar degree of axial tilting between the RET docked pre- and postpowerstroke states is also apparent (Figure 4). Another similarity between these models is the detection of a twisting of the catalytic domain on actin between the pre- and postpowerstroke states.

The most striking differences between the pre- and postpowerstroke states are in the orientations of the neck regions. The RET docking models support the existence of multiple neck-region orientations on actin in the presence of ADP. Variations in neck-region orientations under different strong binding-state conditions has also been reported in EM studies (*26*−*28*). Detectable changes in RET are observed in the presence of phosphate analogues that are most reasonably fit by a neck-region orientation similar to the smooth muscle S1 model. Pre- and postpowerstroke

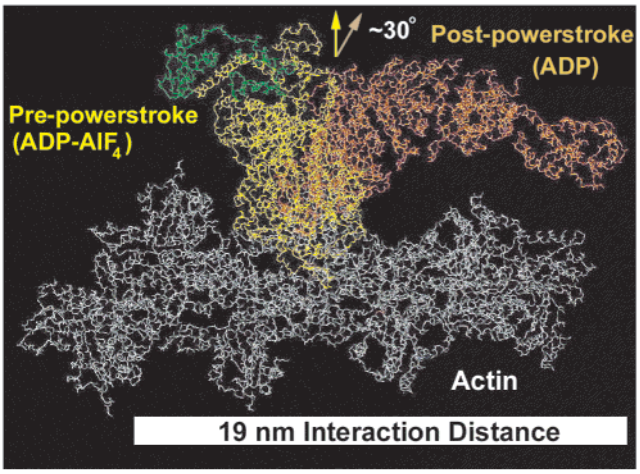

FIGURE 4: Superimposition of the best-fit pre- and postpowerstroke models on the refined actin filament. Note the attachment of the weak-state catalytic domain at an approximately 90° angle followed by tilting over 30°, which contributes several nanometers to the overall displacement between filaments depending on the orientation of the neck region. The combination of neck-region movement and catalytic domain tilting and twisting could produce an interaction distance of up to 19 nm if the crossbridge remains attached to actin for this entire series of conformational changes. The force generating working stroke might be substantially shorter than the interaction distance, so the postpowerstroke conformation shown might easily be removed from actin during rapid filament shortening. This figure was prepared using Maestro software (Schrödinger, Inc., Portland, OR).

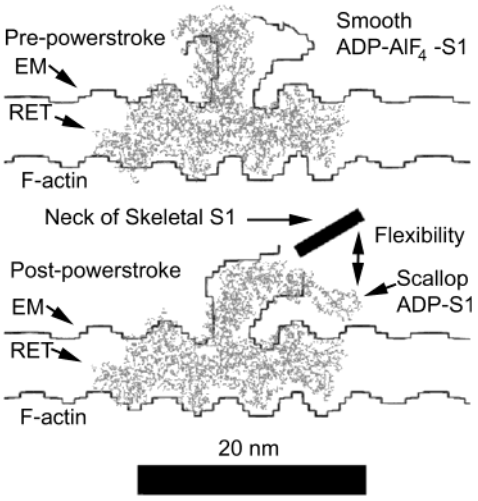

FIGURE 5: Comparisons of the RET docking models with outlines of the published EM images of myosin V on actin. The refined F-actin model was rotated to achieve the best fit within the outlines of the published EM images of myosin V on actin (*11*). The comparison of the models suggests a hypothesis that myosin binds weakly to actin (upper half of figure), followed by a tilting and twisting of the catalytic domain into the postpowerstroke orientations (lower half of figure). A neck-region orientation similar to that in the skeletal muscle S1 atomic model should occur first and might accompany the primary force generating step. The neck-region orientation for skeletal muscle S1 on actin is estimated from alignments of the catalytic domains of skeletal and scallop muscle S1s on actin.

images of myosin V on actin support this large variation in the orientation of the neck region (Figure 5). The RET sensitized emission efficiencies are heavily weighted toward the closest approach of the neck region to the actin filament, so it is not surprising that the RET docked model superimposes well in the catalytic domain region while the neck

Table 4: Interactions at the Acto−S1 Interface between Prepowerstroke and Postpowerstroke Binding[a]

actin myosin[b]	N-terminus		C-terminus		subdomain 2		AA 90−100	
	pre	post	pre	post	pre	post	pre	post
lysine-rich region	++	+	++	o	+	o	++	o
cardiomyopathy loop	++	++	++	o	+	o	+	++
helix−turn−helix	o	+	o	++	o	o	o	++
actin-binding loop 3	o	o	o	+	o	o	o	+
AA 360−371[c]	+	+	o	o	o	o	+	+

[a] Key: (o) α carbons are greater than 1 nm apart; (+) a few potential interactions may occur; (++) several possible interactions are likely. [b] These structures in the myosin catalytic domain are as designated in Figure 2. [c] Recent experimental evidence also supports the influence of actin binding on this C-loop (*46*).

region assumes a location at the end of a distribution of observed neck-region orientations approaching the actin filament.

Comparisons of the myosin V EM images with RET docking yield the most exceptional agreement in the postpowerstroke case, while the RET prepowerstroke state exhibits a greater tilt in the catalytic domain orientation (*11*). One possible interpretation of this difference is that the catalytic domain rotation is a distinct step in a two-stage powerstroke that has already been completed in myosin V when the EM images are taken. The kinetics of myosin V are very different from skeletal muscle myosin, because a large fraction of myosin V is bound in the presence of ATP (*11*). Such kinetic differences may enable distinct stages during the powerstroke to be detected between the two species of myosin, even if the fundamental progression of these stages were similar. Alternatively, differences could arise from the intrinsic biases of the image averaging procedures on EM images versus the use of weighted efficiencies of RET, each of which could affect the docking of an atomic model.

Details of the Acto−S1 Interface during the Pre- to Postpowerstroke Transition. The general structures involved at the acto−S1 interface are similar to those that have already been identified by EM docking models; however, the degree of interaction is somewhat different and varies significantly depending on the pre- or postpowerstroke model. The key regions on S1 and actin that contribute to this interface are summarized in Table 4. The N-terminus, the C-terminus, and amino acids 90−100 of actin make significant contributions to both the pre- and postpowerstroke interfaces. Not surprisingly, the cardiomyopathy loop on S1 also plays a role in both the pre- and postpowerstroke interactions. Variations in this region that induce hypertrophic cardiomyopathy may well be linked to these contacts.

The modeled transition from the pre- to postpowerstroke interfaces agrees well with biochemical and physiological evidence in the literature (*29*, *30*). Table 4 describes how some of the interactions vary between the two models. The most pronounced change is in the contact between the lysine-rich region and the N-terminus of actin in the prepowerstroke model, which decreases in intensity in the postpowerstroke model. This decrease in interaction is in correspondence with mutagenesis, chemical labeling, and antibody competition studies (*31*−*33*). Conversely, the hydrophobic helix−turn−helix of S1 increases its interactions with actin in the postpowerstroke model and correlates with the perturbation of tryptophan fluorescence in single tryptophan mutants (*34*). The limited interaction of the actin binding loop 3 with the region around amino acids 90−100 on actin is supported by mutagenesis studies in Dictyostelium myosin (*35*). Cross-linking of the light chains to actin is also consistent with their close proximity, as found in the scallop muscle S1 model (*36*). Fluorescence polarization reports rotations in the catalytic domain of myosin (*37*). Furthermore, the strong changes in interactions of the actin C-terminus with S1 correlate well with changes in the fluorescence of probes attached to Cys374 on actin (*38*, *39*).

Models of the Actin Filament and Conformational Change. The initial model of the actin filament was based on the G-actin structure as seen in its complex with DNAse I and was later refined in its conformation to improve the fit to X-ray diffraction data (*3*). While previous fluorescenceRET studies have independently verified by docking methods the general validity of these actin filament models (*40*), the fine differences in conformation are significant for the RET docking models proposed here, and their comparisons provide clues to possible structural changes in the actin filament. The RET models based on the refined actin filament produced better fits and structures more consistent with the biochemical and EM data from the literature. This observation suggests that at least some of the features of the refined actin filament model are likely to be representative of the F actin structure, although substantial flexibility in its structural components appears likely.

One of the key differences between the models is in the location of Gln41 in subdomain 2. Although this residue can be chemically cross-linked with Cys374 on an adjacent actin protomer, which is more consistent with the original actin filament model, its location is quite variable in a number of X-ray crystallographic structures of G-actin (*41*). Heterogeneity of this residue's position in the actin filament could increase the observed efficiencies of energy transfer between the myosin nucleotide site and Gln41, because higher RET efficiencies tend to dominate the sensitized emission signal (*42*). Such heterogeneity might even be influenced by the interactions of S1 with actin, so future studies with RET measurements between additional probe labeling sites on actin and S1 might clarify the precise nature of such induced structural changes and refine the current models.

Implications for Conformational Selection. Previous reports have indicated that the dissociated myosin head has a broad distribution of neck-region orientations with respect to the catalytic domain rather than a single precocked orientation (*8*, *43*, *44*). Our conformational selection hypothesis proposed that one of these conformations would preferentially bind to actin in an orientation that would allow conversion to the strong binding state (*8*). The docking model of the prepowerstroke state suggests that a neck-region orientation similar to the smooth muscle S1 atomic model is preferentially detected in the RET data. These results support our conformational selection hypothesis that describes an important structural transition enabling the subsequent development of force at the molecular level.

The accuracy and precision of the docking models generated based on RET depend on the appropriateness of the atomic models of S1 and F actin that are available. The atomic models of smooth muscle S1 and scallop muscle ADP−S1 that fit the pre- and postpowerstroke data best,

respectively, represent structures that contain what are presumed to be the most extreme orientations of the neck region with respect to their approach to the actin filament. Therefore, the RET data will be biased toward their detection. Evidence from EM suggests it is unlikely that models with more extreme neck-region orientations than those examined here will be uncovered. Also, a broader range of RET measurements produce further constraints on the modeling process. A number of conventional RET measurements in the literature between actin and S1 in the postpowerstroke state agree with the models presented here, especially when the precision of the orientation factor is considered (*12*). These results help to confirm the proposed models.

In summary, the molecular models of the pre- and postpowerstroke states of S1 on actin are consistent with a number of biochemical and EM observations, although some of the specific interactions suggested by EM docking models have been refined. The results are in agreement with models predicting that the X-ray crystallographic structures of smooth muscle S1 represent a prepowerstroke conformation (*5*). The models suggest an interesting progression of events in which both the catalytic domain and the neck region of myosin contribute toward the axial rotations of approximately 30° that displace the actin filament relative to myosin in a manner not unlike those generally described from the electron paramagnetic resonance studies of scallop muscle and EM of insect flight muscle (*9*, *10*) or from previous studies of purified skeletal S1 interacting with actin (*45*). Further refinement of the RET model will provide more information on specific structural changes in the actin filament during this fundamental molecular cycle that plays such an important role in life processes and disease.

ACKNOWLEDGMENT

We thank Dr. Julian Borejdo for his comments on the manuscript. Dr. Michael Lorenz kindly provided us with the coordinates for the refined model of F actin and their docking to S1.

REFERENCES

1. Holmes, K. C., Popp, D., Gebhard, W., and Kabsch, W. (1990) *Nature 347*, 44−49.
2. Rayment, I., Holden, H. M., Whittaker, M., Yohn, C. B., Lorenz, M., Holmes, K. C., and Milligan R. A. (1993) *Science 261*, 58−65.
3. Lorenz, M., Popp, D., and Holmes, K. C. (1993) *J. Mol. Biol. 234*, 826−836.
4. Mendelson, R., and Morris, E. P. (1997) *Proc. Natl. Acad. Sci. U.S.A. 94*, 8533−8538.
5. Dominguez, R., Freyzon, Y., Trybus, K. M., and Cohen, C. (1998) *Cell 94*, 559−571.
6. Houdusse, A., Kalabokis, V. N., Himmel, D., Szent-Györgyi, A. G., and Cohen, C. (1999) *Cell 97*, 459−470.
7. Houdusse, A., Szent-Györgyi, A. G., and Cohen, C. (2000) *Proc. Natl. Acad. Sci. U.S.A. 97*, 11238−11243.
8. Xu, J., and Root, D. D. (2000) *Biophys. J. 79*, 1498−1510.
9. Baker, J. E., Brust-Mascher, I., Ramachandran, S., LaConte, L. E., and Thomas, D. D. (1998) *Proc. Natl. Acad. Sci. U.S.A. 95*, 2944−2949.
10. Taylor, K. A., Schmitz, H., Reedy, M. C., Goldman, Y. E., Franzini-Armstrong, C., Sasaki, H., Tregear, R. T., Poole, K., Lucaveche, C., Edwards, R. J., Chen, L. F., Winkler, H., and Reedy, M. K. (1999) *Cell 99*, 421−431.
11. Walker, M. L., Burgess, S. A., Sellers, J. R., Wang, F., Hammer, J. A., III, Trinick, J., and Knight, P. J. (2000) *Nature 405*, 804−807.
12. dos Remedios, C. G., Miki, M., and Barden, J. A. (1987) *J. Muscle Res. Cell Motil. 8*, 97−117.
13. Saraswat, L. D., and Lowey, S. (1998) *J. Biol. Chem. 273*, 17671−17679.
14. Xu, J., and Root, D. D. (1998) *J. Struct. Biol. 123*, 150−161.
15. Godfrey, J., and Harrington, W. F. (1970) *Biochemistry 9*, 886−895.
16. Weeds, A. G., and Pope, B. (1977) *J. Biol. Chem. 111*, 129−157.
17. Wagner, P. D. (1982) *Methods Enzymol. 85*, 72−81.
18. Root, D. D. (1997) *Proc. Natl. Acad. Sci. U.S.A. 91*, 5685−5690.
19. Kim, E., Miller, C. J., Motoki, M., Seguro, K., Muhlrad, A., and Reisler, E. (1996) *Biophys. J. 70*, 1439−1446.
20. Root, D. D., Shangguan, X., Xu, J., and McAllister, M. (1999) *J. Struct. Biol. 127*, 22−34.
21. Selvin, P. R., and Hearst, J. E. (1994) *Proc. Natl. Acad. Sci. U.S.A. 91*, 10024−10028.
22. Mornet, D., Bertrand, R., Pantel, P., Audemard, E., and Kassab, R. (1981) *Nature 292*, 301−306.
23. Sutoh, K. (1982) *Biochemistry 21*, 3654−3661.
24. Vandekerckhove, J., Deboben, A., Nassal, M., and Wieland, T. (1985) *EMBO J. 4*, 2815−2818.
25. Root, D. D., and Reisler, E. (1992) *Biophys. J. 63*, 730−740.
26. Whittaker, M., Wilson-Kubalek, E. M., Smith, J. E., Faust, L., Milligan, R. A., and Sweeney, H. L. (1995) *Nature 378*, 748−751.
27. Jontes, J. D., Wilson-Kubalek, E. M., and Milligan, R. A. (1995) *Nature 378*, 751−753.
28. Carragher, B. O., Cheng, N., Wang, Z. Y., Korn, E. D., Reilein, A., Belnap, D. M., Hammer, J. A., III, and Steven, A. C. (1998) *Proc. Natl. Acad. Sci. U.S.A. 95*, 15206−15211.
29. dos Remedios, C. G., and Moens, P. D. (1995) *Biochim. Biophys. Acta 1228*, 99−124.
30. Cooke, R. (1997) *Physiol. Rev. 77*, 671−697.
31. Cook, R. K., Root, D. D., Miller, C., Reisler, E., and Rubinstein, P. A. (1993) *J. Biol. Chem. 268*, 2410−2415.
32. Bertrand, R., Chaussepied, P., Audemard E., and Kassab, R. (1989) *Eur. J. Biochem. 181*, 747−754.
33. DasGupta, G., and Reisler, E. (1992) *Biochemistry 31*, 1836−1841.
34. Yengo, C. M., Fagnant, P. M., Chrin, L., Rovner, A. S., and Berger, C. L. (1998) *Proc. Natl. Acad. Sci. U.S.A. 95*, 12944−12949.
35. Razzaq, A., Schmitz, S., Veigel, C., Molloy, J. E., Geeves, M. A., and Sparrow, J. C. (1999) *J. Biol. Chem. 274*, 28321−28328.
36. Andreeva, A. L., Andreev, O. A., and Borejdo, J. (1993) *Biochemistry 32*, 13956−13960.
37. Burghardt, T. P., Garamszegi, S. P., and Ajtai, K. (1997) *Proc. Natl. Acad. Sci. U.S.A. 94*, 9631−9636.
38. Crosbie, R. H., Chalovich, J. M., and Reisler, E. (1992) *Biochem. Biophys. Res. Commun. 184*, 239−245.
39. Root, D. D., and Wang, K. (2001) *Biochemistry 40*, 1171−1186.
40. Miki, M., O'Donoghue, S. I., and dos Remedios, C. G. (1992) *J. Muscle Res. Cell Motil. 13*, 132−145.
41. Kim, E., Wriggers, W., Phillips, M., Kokabi, K., Rubenstein, P. A., and Reisler, E. (2000) *J. Mol. Biol. 299*, 421−429.
42. Heyduk, T., and Heyduk, E. (2001) *Anal. Biochem. 289*, 60−67.
43. Palm, T., Sale, K., Brown, L., Li, H., Hambly, B., and Fajer, P. G. (1999) *Biochemistry 38*, 13026−13034.
44. Shih, W. M., Gryczynski, Z., Lakowicz, J. R., and Spudich, J. A. (2000) *Cell 102*, 683−694.
45. Pollard, T. D., Bhandari, D., Maupin, P., Wachsstock, D., Weeds, A. G., and Zot, H. G. (1993) *Biophys. J. 64*, 454−471.
46. Ajtai, K., Garamszegi, S. P., Park, S., Velazquez Dones, A. L., and Burghardt, T. P. (2001) *Biochemistry. 40*, 12078−12093.

BI015869O